

EE 475 Final Project
Vision-Based Autonomous Navigation Assistance
Boğaziçi University Campus Route

Enes Kuzuoglu
Mehmet Emin Algül

Introduction

This project develops a computer vision-based navigation assistance system for an autonomous shuttle operating between Boğaziçi University's North and South Campuses. The work focuses on real-world challenges such as varying illumination, worn lane markings, and asphalt irregularities. By applying classical image processing techniques from Gonzalez and Woods, the system aims to create reliable modules for lane tracking, traffic light classification, obstacle detection and barrier-state detection in unstructured environments.

1 Methods and Materials

1.1 Lane Detection and Tracking

The lane detection module employs a hybrid segmentation approach designed to function robustly under varying illumination conditions. The pipeline consists of three stages: feature extraction via morphological and chromatic fusion, geometric modeling using the Hough Transform, and temporal tracking.

1.1.1 Hybrid Feature Extraction

To isolate lane markings, we implement a logical disjunction of two masking techniques. First, a chromatic mask M_{color} is generated in the HSV space, targeting white, yellow, and a specific shadow-invariant subspace defined as $H \in [108, 130]$, $S \in [45, 52]$. Simultaneously, a morphological Top-Hat transform is applied to the grayscale image I_{gray} using a 19×19 rectangular kernel S to isolate high-contrast local structures:

$$I_{TH} = I_{gray} - (I_{gray} \circ S) \quad (1)$$

The final binary mask M_{final} is the union of the chromatic and morphological masks[2].

1.1.2 Geometric Extraction via Hough Transform

Edge detection is performed on M_{final} using the Canny operator. To detect linear lane boundaries from the resulting edge map, we utilize the **Probabilistic Hough Transform (PHT)**. Unlike the standard Cartesian representation ($y = mx + b$), the Hough Transform parameterizes lines in polar coordinates to avoid singularities with vertical lines: [4]

$$\rho = x \cos \theta + y \sin \theta \quad (2)$$

where ρ is the perpendicular distance from the origin to the line, and θ is the angle of the normal vector. Each edge pixel (x, y) in the image space votes for potential sinusoidal curves in the (ρ, θ) parameter space. The PHT optimization minimizes computational cost by analyzing a random subset of points to detect line segments defined by endpoints $P = \{(x_1, y_1), (x_2, y_2)\}$. Segments with slopes $|\frac{dy}{dx}| < 0.4$ are rejected as environmental noise.

1.1.3 Temporal Tracking and Stabilization

Detected line segments are organized into *Lane Candidates*. A candidate state \mathbf{l}_t is updated using an Exponential Weighted Moving Average (EWMA) filter for temporal smoothness:

$$\mathbf{l}_t = \alpha \cdot \mathbf{l}_{new} + (1 - \alpha) \cdot \mathbf{l}_{t-1} \quad (3)$$

with $\alpha = 0.7$. A hysteresis filter confirms a lane only after $N_{min} = 8$ consecutive detections and retains it in memory for $N_{miss} = 5$ frames during temporary occlusions.

1.2 Barrier Position Detection

To robustly distinguish barrier states, we employ a sensor-fusion approach that validates geometric structure with chromatic signatures, effectively filtering background noise.

1.2.1 Geometric Structure Extraction

Vertical gradients are extracted from the grayscale ROI, I_{gray} , to isolate horizontal edges. The gradient G_y is computed via convolution with the Sobel-Y kernel K_y :

$$G_y = I_{gray} * K_y \quad \text{where} \quad K_y = \begin{bmatrix} -1 & -2 & -1 \\ 0 & 0 & 0 \\ +1 & +2 & +1 \end{bmatrix} \quad (4)$$

The gradient magnitude is thresholded to form an edge map. To reconstruct the barrier's physical body from disjoint edges, we apply morphological dilation using an anisotropic rectangular structuring element S_{rect} (5×15 pixels):

$$M_{struct} = M_{edge} \oplus S_{rect} \quad (5)$$

1.2.2 Logic-Gated Verification

Simultaneously, chromatic masks M_{red} and M_{white} are generated in HSV space. To ensure spatial coherence, we calculate the pixel count of color features strictly *within* the structural mask:

$$N_{red} = |M_{red} \cap M_{struct}| \quad , \quad N_{white} = |M_{white} \cap M_{struct}| \quad (6)$$

The barrier is classified as **CLOSED** only if the geometric structure and both spectral components simultaneously exceed their respective thresholds τ :

$$State = \begin{cases} \text{CLOSED} & \text{if } (|M_{struct}| > \tau_S) \wedge (N_{red} > \tau_R) \wedge (N_{white} > \tau_W) \\ \text{OPEN} & \text{otherwise} \end{cases} \quad (7)$$

1.3 Traffic Light Detection and Classification

Traffic light detection is formulated as a constrained color-segmentation problem followed by geometric validation. Each frame $I(x, y)$ is mapped from RGB to HSV space, where

chromatic components are less sensitive to illumination variations. A fixed Region of Interest (ROI) $\Omega_{\text{TL}} \subset I$ is defined based on prior geometric knowledge of traffic light placement.

For each color class $k \in \{\text{red}, \text{yellow}, \text{green}\}$, a binary mask is obtained via thresholding

$$M_k(x, y) = \begin{cases} 1, & \text{if } (H, S, V) \in \mathcal{T}_k \\ 0, & \text{otherwise} \end{cases}$$

where \mathcal{T}_k denotes the HSV threshold set for class k . Morphological opening is applied to M_k to suppress small-scale noise. Connected components are extracted, and each candidate region \mathcal{R} is evaluated using its area A , mean brightness [6]

$$\bar{V} = \frac{1}{|\mathcal{R}|} \sum_{(x,y) \in \mathcal{R}} V(x, y),$$

and circularity

$$C = \frac{4\pi A}{P^2},$$

where P is the contour perimeter. Frame-level decisions are temporally stabilized using majority voting over a finite window $\{t - N, \dots, t\}$.

1.4 Obstacle Detection

Obstacle detection is treated as a structural anomaly detection problem using spatial edge statistics. After Gaussian smoothing, Canny edge detection is applied to obtain a binary edge map $E(x, y)$. Processing is restricted to a road-region ROI Ω_{obs} .

The edge map is partitioned into N vertical bins $\{B_i\}_{i=1}^N$, and column-wise edge density is computed as

$$d_i = \sum_{(x,y) \in B_i} E(x, y).$$

Bins satisfying

$$d_i > \mu_d + \alpha \sigma_d$$

are selected as candidates, where μ_d and σ_d denote the mean and standard deviation of $\{d_i\}$. For each candidate region, vertical localization is refined using row-wise edge accumulation

$$r(y) = \sum_x E(x, y),$$

yielding a bounding box constrained by geometric conditions on width, height, and aspect ratio. To enforce temporal consistency, detections are confirmed only if they persist across multiple frames using a sliding-window voting rule.

2 Results

2.1 Performance Evaluation Metrics

To rigorously assess the discrete classification tasks (barrier state and lane presence), we utilize standard statistical metrics derived from the confusion matrix elements: True Positives (TP), True Negatives (TN), False Positives (FP), and False Negatives (FN). The system's reliability is quantified using Accuracy, Precision, Recall, and the F1-Score, defined as follows:

$$\begin{aligned} \text{Accuracy} &= \frac{TP + TN}{TP + TN + FP + FN} & \text{Precision} &= \frac{TP}{TP + FP} \\ \text{Recall} &= \frac{TP}{TP + FN} & \text{F1-Score} &= 2 \cdot \frac{\text{Precision} \cdot \text{Recall}}{\text{Precision} + \text{Recall}} \end{aligned} \quad (8)$$

These metrics provide a comprehensive view of the algorithmic performance, isolating geometric misclassifications from chromatic validation errors.

2.2 Lane Detection and Tracking Performance

The lane detection module, was evaluated for its performance in challenging conditions including varied lighting and shadows. While precise quantitative accuracy metrics are difficult to establish due to the continuous nature of lane presence and the inherent variability in road markings, the system consistently demonstrated robust lane identification. Qualitative results from diverse scenarios are presented in Figure 1. These images highlight the system's ability to detect and track lane boundaries effectively, even in the presence of significant illumination changes and partial occlusions.



(a) Detection in standard daylight



(b) Detection under varying light

Figure 1: Performance of the Hybrid Lane Detection system under varying environmental conditions.

2.3 Barrier State Detection Performance

The classification performance was evaluated across three annotated video sequences. On this test set, the system achieved a **Precision** of 100% and a **Recall** of 100%, resulting in a perfect

F1-Score of 1.0. These metrics quantitatively confirm that the logical fusion of geometric and chromatic features effectively eliminated False Positives (FP) caused by background clutter while maintaining maximum sensitivity to the barrier structure. Qualitative results are illustrated in Figure 2.



(a) Detected "Closed" State

(b) Detected "Open" State

Figure 2: Qualitative results of the Barrier Position Detection module on test data.

2.4 Traffic Light Detection and Classification Performance

The traffic signal recognition module was evaluated on a dataset containing 10 active traffic lights. The system demonstrated perfect sensitivity, successfully detecting all instances ($TP = 10$, $FN = 0$), yielding a **Recall of 100%**. This confirms the system's safety-critical reliability, ensuring no signals were missed.

However, the geometric filtering stage exhibited a tendency to over-segment, identifying 5 circular traffic signs as signal lights ($FP = 5$). Consequently, the **Precision** was calculated at 66.7%, resulting in an overall **F1-Score of 0.80**. Although the False Positive rate reduces precision, the design philosophy prioritizes Recall to absolutely eliminate the hazardous risk of failing to detect a stop signal. Detection results are visualized in Figure 3.



Red Light



Yellow Light



Green Light



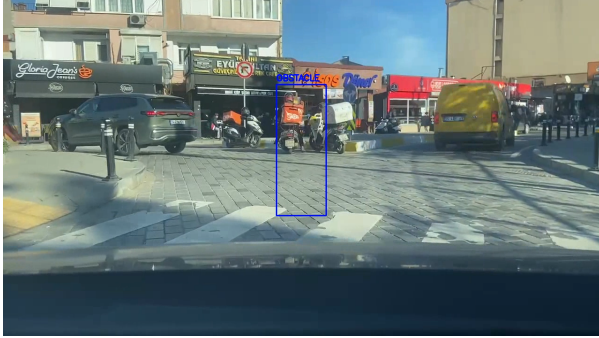
False Positive

Figure 3: Representative traffic light detection results.

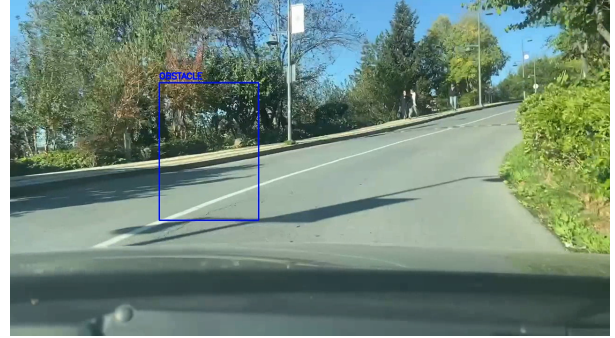
2.5 Obstacle Detection

The obstacle detection subsystem was evaluated on a test sequence yielding 60 total detection events. Analysis against ground truth data revealed 45 True Positives (TP) and 15 False Positives (FP), while 5 actual obstacles were missed ($FN = 5$).

This performance results in a **Precision of 75.0%**, indicating a moderate rate of false alarms caused by complex background textures. However, crucial for autonomous safety, the system achieved a high **Recall of 90.0%**, ensuring the majority of physical hazards were correctly identified. The overall algorithmic balance is reflected in an **F1-Score of 0.82**. Representative detection results are shown in Figure ??.



(a) Correct detection: Motorcycle



(b) False Positive: Background noise

Figure 4: Qualitative evaluation of the Obstacle Detection module.

3 Discussion

The results highlight a clear performance dichotomy between structural and semantic tasks. The **Barrier** and **Lane** modules demonstrated superior robustness against environmental noise (shadows) compared to standard edge detection, evidenced by the barrier’s perfect F1-Score (1.0). However, the **Traffic Light** and **Obstacle** modules revealed the deficiencies of classical geometric methods. While achieving high Recall to ensure safety, their lower Precision (66.7% and 75% respectively) indicates an inability to distinguish semantically similar objects (e.g., traffic signs vs. signals) without the learned features inherent to Deep Learning approaches, resulting in a higher rate of false alarms.

4 Conclusion

This project successfully validated a real-time classical perception stack while identifying key precision limitations. Future work will integrate a lightweight CNN to classify traffic light candidates, directly addressing the high false-positive rate noted in the discussion. Additionally, Optical Flow algorithms will be implemented to distinguish moving hazards from static background textures, improving obstacle detection precision. Finally, Inverse Perspective Mapping (IPM) will be adopted to linearize lane geometry for better curvature handling.

Bibliography

References

- [1] Gonzalez, R. C., and Woods, R. E., *Digital Image Processing*, 4th ed., Pearson, 2018.
- [2] Parajuli, A., Çelenk, M., and Riley, H. B., “Robust Lane Detection in Shadows and Low Illumination Conditions using Local Gradient Features,” *Open Journal of Applied Sciences*, vol. 3, pp. 68–74, 2013.
- [3] Du, M., Wang, J., Li, N., and Li, D., “Shadow Lane Robust Detection by Image Signal Local Reconstruction,” *IJSPIPR*, vol. 9, no. 3, pp. 89–102, 2016.
- [4] Hough, P. V. C., “Method and Means for Recognizing Complex Patterns,” U.S. Patent 3,069,654, 1962.
- [5] Duda, R. O., and Hart, P. E., “Use of the Hough Transformation to Detect Lines and Curves in Pictures,” *Communications of the ACM*, vol. 15, no. 1, pp. 11–15, 1972.
- [6] Omachi, M., and Omachi, S., “Traffic Light Detection with Color and Edge Information,” Proc. *IEEE Cimsa*, pp. 284–287, 2009.
- [7] Chae, S., Kim, S., and Pan, S., “Traffic Light Detection Algorithm based on Color and Shape Information,” *Journal of the KITE*, vol. 41, pp. 35–42, 2004.
- [8] Soille, P., *Morphological Image Analysis*, Springer, 2003.
- [9] Bai, X., and Zhou, F., “Analysis of New Top-Hat Transformation and the Application for Infrared Small Target Detection,” *Pattern Recognition Letters*, vol. 31, no. 14, pp. 2143–2152, 2010.